THE EUROPEAN
PHYSICAL JOURNAL B

On symmetric breather collisions in lattices with saturable nonlinearity

A. Maluckov[1,a], Lj. Hadžievski[2], and M. Stepić[3]

[1] Faculty of Sciences and Mathematics, University of Niš, P.O. Box 224, 18001 Niš, Serbia
[2] Vinča Institute of Nuclear Sciences, P.O. Box 522, 11001 Belgrade, Serbia
[3] Institute of Physics and Physical Technologies, Clausthal University of Technology, 38678 Clausthal-Zellerfeld, Germany

Abstract. Symmetric collisions of two discrete breathers in the lattice with saturable nonlinearity are investigated. The strong correlation of the collision properties and the parameters of colliding breathers (power, velocity, and phase difference), lattice parameters and position of the collision point is found. This is related to the internal structure of the colliding breathers and energy exchange with the phonon background. The type of collision changes from elastic to the inelastic (the breathers merging, multi-bounce interactions, breather creation etc.) with the increasing of the colliding breather power. Collision of high power breathers always results in the breather fusion. The elastic and inelastic collisions are related to the periodic and quasi-periodic colliding breathers, respectively.

PACS. 42.65.Tg Optical solitons; nonlinear guided waves – 63.20.Pw Localized modes

1 Introduction

Investigation of the localized mode interactions is one of the central topics of the nonlinear dynamics. It may find applications in photonics (all-optical switching, steering, [1,2]), in biological phenomena (denaturation of DNA [3,4]), in the physics of Bose-Einstein condensates (matter wave soliton applications [5,6]), etc. In integrable systems soliton collisions are elastic, i.e. the colliding solitons are not affected by the collisions. On the contrary, in nonintegrable systems various inelastic effects such as trapping and formation of bound states, multi-bounce interactions [7], fractality in the collision output [8], etc. are possible. This diversity is usually associated with the internal structure of colliding localized modes [9], and their mutual radiationless energy exchange [1,10].

Interactions of the localized modes are closely related to the existence of moving localized modes. In continuous nonlinear media, as a consequence of the continuous translational invariance, moving localized modes can be initiated at an arbitrary position and with an arbitrary transverse velocity. However, in discrete nonlinear media, the discreteness breaks translational invariance of the corresponding continuous system. As a consequence, moving discrete localized modes can be created only at some positions in the lattice and with transverse velocities within

some defined intervals. In particular, in lattices with saturable nonlinearity, the localized mode of breather type with high power exists only for a few values of the total power and transverse velocity [11–13].

While interactions of the localized modes in continuous systems with saturable nonlinearity are extensively studied [14,15], this is not a case with the corresponding interactions of discrete localized modes [16]. Therefore, in this paper, the collisions of discrete breathers in lattices with saturable nonlinearity [11,12,16] are studied. Collision properties in the discrete systems with saturable nonlinearity are compared with the collision properties in the discrete systems with other types of nonlinearity [1], and in continuous systems with saturable nonlinearity [14,15] and power low nonlinearity [17]. In Section 2, brief overview of the one-dimensional DNLS lattice model with saturable nonlinearity is presented. The breather internal structure and characteristics of the breather dynamics are indicated by the perturbation approach. The existence and stability of bright moving breathers are discussed in Section 3. Regarding stability two approaches are exploited: the dynamical and mapping stability analysis. In Section 4, the correspondence of the interaction properties, the internal structure and the dynamics of the colliding breathers, is studied using Fourier analysis. Correlation of the collision properties and the system parameters (total power, breathers transverse

[a] e-mail: maluckov@junis.ni.ac.yu

velocity, and the position of the collision center) is discussed. Conclusions are summarized in Section 5.

2 Model

The one-dimensional DNLS lattice model with saturable nonlinearity [11,12] is given by

$$i\frac{dU_n}{dt} + (U_{n+1} + U_{n-1} - 2U_n) - \gamma\frac{U_n}{1+|U_n|^2} = 0, \quad (1)$$

where U_n is the wave function in the nth lattice element $(n = 1,...N)$ with periodic boundary conditions, $(U_{N+1} = U_1)$, and γ is the nonlinearity parameter. Equation (1) represents a system of linearly coupled nonlinear difference-differential equations which are not integrable. Here, three integral quantities of interest for the future analysis are power P, Hamiltonian H and momentum Q

$$P = \sum_n |U_n|^2, \quad (2)$$

$$H = \sum_n [\gamma \ln(1 + |U_n|^2) + |U_{n-1} - U_n|^2], \quad (3)$$

$$Q = \frac{i}{2}\sum_n (U_{n+1}^* U_n - U_n^* U_{n+1}). \quad (4)$$

The P and H are conserved as a consequence of the system invariance with respect to the phase shift and time shift, respectively. Due to the symmetry breaking caused by the lattice discreteness, the system is not invariant with respect to the spatial translations. Consequently, momentum Q is not conserved [18].

The stationary solution to equation (1) is of the form

$$U_n(t) = \phi_n(\omega)e^{-i\omega t}, \quad (5)$$

where ω is the propagation parameter. The resulting set of coupled algebraic equations for the real function ϕ_n [12], after some simple algebra, coincides with the stationary generalized discrete nonlinear Schrödinger (GDNLS) equation [19,20] $(V = 1, \mu = 1)$

$$(\omega - 2 - \gamma)\phi_n + (\phi_{n+1} + \phi_{n-1})(1 + \phi_n^2) + (\omega - 2)\phi_n^3 = 0. \quad (6)$$

At the value $\omega = 2$, the equation (6) is the stationary version of the discrete, integrable Ablowitz-Ladik equation [21].

Previous investigations [11–13] have confirmed the existence of two types of bright stationary solitons with a single maximum in a lattice. These are the on-site soliton, centered at the lattice element, and inter-site soliton, centered between two neighboring lattice elements [22]. The bright solitons exist in the parameter range $\omega \leq \gamma$. Between two coexisting modes with the fixed power, the stable mode is characterized with lower energy. This is confirmed by the dynamical and mapping stability analysis [13]. Moving localized mode can be generated by transversely kicking the unstable stationary mode. The resulting moving localized mode of the breather type has the same power as the corresponding stationary mode. An analytical proof of the stability of moving breathers is still a challenge [23–25].

2.1 Perturbational approach

The dynamics close to the solution ϕ_n, equation (5), can be described by introducing the perturbation expansion [18]

$$U_n(t) = [\phi_n + \lambda\epsilon_n(t) + \lambda^2\nu_n(t) + ...]\exp(-i\omega t), \quad (7)$$

where λ is a small expansion parameter, and ϵ_n, ν_n are perturbation terms in a frame rotating with the frequency ω. Note that generally a slow time dependence of the parameter ω can be allowed as in [18]. After substituting the expansion (7) into (1) and identifying coefficients for consecutive powers of λ, the zeroth order equation coincides with (6), while the first and second order equations can be written as

$$i\dot{\epsilon}_n + (\omega - 2)\epsilon_n + \epsilon_{n+1} + \epsilon_{n-1} - \gamma\frac{\epsilon_n - \phi_n^2\epsilon_n^*}{(1+\phi_n^2)^2} = 0, \quad (8)$$

$$i\dot{\nu}_n + (\omega - 2)\nu_n + \nu_{n+1} + \nu_{n-1}$$
$$- \gamma\frac{\nu_n - \phi_n^2\nu_n^* - 2\phi_n|\epsilon_n|^2 - \epsilon^2\phi_n}{(1+\phi_n^2)^2} = 0. \quad (9)$$

The zeroth, first and second order equations describe the breather shape, behavior of the small breather perturbations, and long-time behavior of the perturbed breather, respectively [18].

The dynamics of breather perturbations can be considered following the approach used in [18], established for the DNLS model with cubic nonlinearity. The substitution in the form

$$\epsilon_n(t) = \frac{1}{2}a(V_n + W_n)\exp(-i\omega_p t)$$
$$+ \frac{1}{2}a^*(V_n^* - W_n^*)\exp(i\omega_p t), \quad (10)$$

gives

$$\omega_p V_n = -(\omega - 2)W_n - W_{n+1} - W_{n-1} + \gamma\frac{W_n}{1+\phi_n^2}$$
$$\equiv \mathsf{L}_0\{W_n\}, \quad (11)$$

$$\omega_p W_n = -(\omega - 2)V_n - V_{n+1} - V_{n-1} + \gamma\frac{(1-\phi_n^2)V_n}{(1+\phi_n^2)^2}$$
$$\equiv \mathsf{L}_1\{V_n\}, \quad (12)$$

or in matrix form

$$\mathsf{M}^{(0)}\begin{bmatrix}\{V_n\}\\\{W_n\}\end{bmatrix} = \begin{bmatrix}0 & \mathsf{L}_0\\\mathsf{L}_1 & 0\end{bmatrix}\begin{bmatrix}\{V_n\}\\\{W_n\}\end{bmatrix} = \omega_p\begin{bmatrix}\{V_n\}\\\{W_n\}\end{bmatrix}. \quad (13)$$

Vector $(\{V_n\}, \{-iW_n\})$ is the eigenvector of the corresponding Floquet matrix with the eigenvalue $\exp(i\omega_p T)$, where the period T is arbitrary due to the time independence of the coefficients in (11) and (12), [18]. The spectrum of non-Hermitian matrix $\mathsf{M}^{(0)}$ can be divided into the continuous (phonon) part, corresponding to extended eigenvectors, and discrete part, corresponding to the breather internal modes. The phonon spectrum for any perturbed localized solution ϕ_n can be derived from the

limit $|n| \to \infty$, since the condition $\phi_n \to 0$ reduces system (11), (12) into two uncoupled equations for $V_n + W_n$ and $V_n - W_n$. Assuming $V_n \pm W_n \approx \exp(\pm iq_\pm n)$, two dispersion relations are obtained

$$\omega_p = \pm(\omega - 2 - \gamma) \mp 2\cos(q). \tag{14}$$

The phonon spectrum consists of two branches, $|\omega_p| \epsilon [\gamma - \omega, \gamma - \omega + 4]$, symmetrically located around $\omega_p = 0$, which never overlap. Two eigenvectors correspond to the same solution of equation (13). Therefore, only $\omega_p > 0$ is considered. Spatially localized eigensolutions associated with the eigenvalues outside the phonon spectrum, interacting with the unperturbed soliton, can excite internal modes.

The equation (9) gives possibility to consider the long-time behavior of the localized mode in the presence of perturbations. The terms on the righthand side containing the second order of ϵ describe the interactions between modes [18,24]. Substitution of the expansion (10) into (9) (assuming ϕ_n, V_n, W_n are real [18]) gives the following equation

$$
\begin{aligned}
L(\omega)\nu_n = &-\frac{\gamma\phi_n}{2}(3V_n^2 + W_n^2)|a|^2 \\
&+ \frac{\gamma\phi_n}{2}\left[(3V_n^2 - W_n^2)\text{Re}(a^2 e^{-2i\omega_p t})\right] \\
&+ \frac{2iV_n W_n \gamma\phi_n}{2}\text{Im}(a^2 e^{-2i\omega_p t}).
\end{aligned}
\tag{15}
$$

The righthand side of equation (15) contains a static part, and a part involving frequencies $\pm 2\omega_p$. When $2|\omega_p|$ is inside the phonon band of the perturbed solution, a resonance occurs resulting in the energy exchange between breather and phonon band. On the other hand, when $2|\omega_p|$ is in the discrete part of perturbed solution spectrum, the resonance can excite a new internal oscillation of the localized mode. Similar reasoning can be extended to the higher order equations with respect to the small perturbation (see the beginning of this section) [18].

The phonon-breather interaction (the breather radiates or absorbs energy from the background), and the breather interaction with discrete part of perturbation spectrum are main mechanisms for the excitation of the internal mode dynamics of the breather [9], which is observed in the numerical experiments.

2.2 Numerical approach

The numerical model is based on the 6th order Runge-Kutta procedure. Most of the results presented here are obtained for fixed value of the parameter $\gamma = 9.1$ [12,13], laying inside the domain where the cascade saturation mechanism is significant. The transverse motion is initiated by adding the phase term to the stationary soliton, $U_n \to U_n \exp(i\,k\,n)$, where k is the transverse velocity parameter. In order to initialize the symmetric collision of two solitons they are directed at each other, i.e. $k_1 = k$ and $k_2 = -k$, where indices note the colliding modes.

The power spectrum (the spectrum of $\text{Re}(U_{nc}(t))$, where at nc the amplitude is maximal) and the amplitude
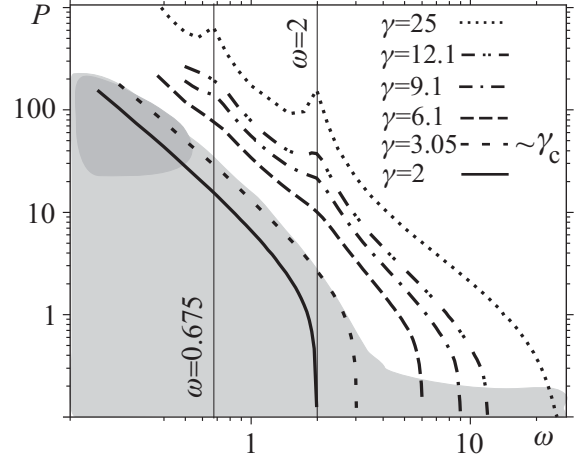

Fig. 1. The total power of on-site localized modes as a function of parameter ω for different γ in log-log proportion. The moving breathers are observed for the critical values of parameter ω, i.e. at turning points (straight lines), and in the gray region.

spectrum (the spectrum of $|U_{nc}(t)|$), are calculated with IMSL subroutine based on the fast-Fourier technique [26].

3 Moving localized modes

Particularity of the systems with saturable nonlinearity (continuous and discrete), in comparison to the systems with cubic nonlinearity, is the cascade mechanism of the amplitude saturation [12,17]. This mechanism becomes significant in the lattice parameter range $\gamma > \gamma_c$, where γ_c corresponds to the critical $P(\omega)$ curve in Figure 1. In this region ($\gamma > \gamma_c$), the moving localized mode of high power can be obtained by transversely kicking the corresponding unstable stationary localized mode, Figures 1 and 2. The previous results concerning the cascade mechanism for amplitude saturation are briefly commented in the next part of this section.

Initially, the stationary localized discrete mode is a soliton (without internal structure), but the corresponding transversely moving discrete mode is a breather with characteristic internal frequencies. This is a direct consequence of the system discreteness and the breaking of the continuous translational invariance in the lattice systems as indicated by the non-conservation of Q [1]. It is confirmed numerically in the reference [12]. The symmetry breaking can be associated with the creation of the Peierls-Nabarro potential barrier to the localized mode transverse motion [2,27]. The trapped - moving localized mode bifurcation is dependent on the system parameters, as shown in Figures 1 and 2.

In the lattice with saturable nonlinearity, the moving breathers with high power are found only for a few values of the parameters P and k, contrary to the corresponding continuous case. More precisely, a bifurcation trapped-moving mode, in a lattice with saturable nonlinearity, is observed in some ranges of k at $\omega = 2\,(P = 21.63)$, $\omega = 1.05\,(P = 64.03)$, $\omega = 0.675\,(P = 140.56)$ as noted in
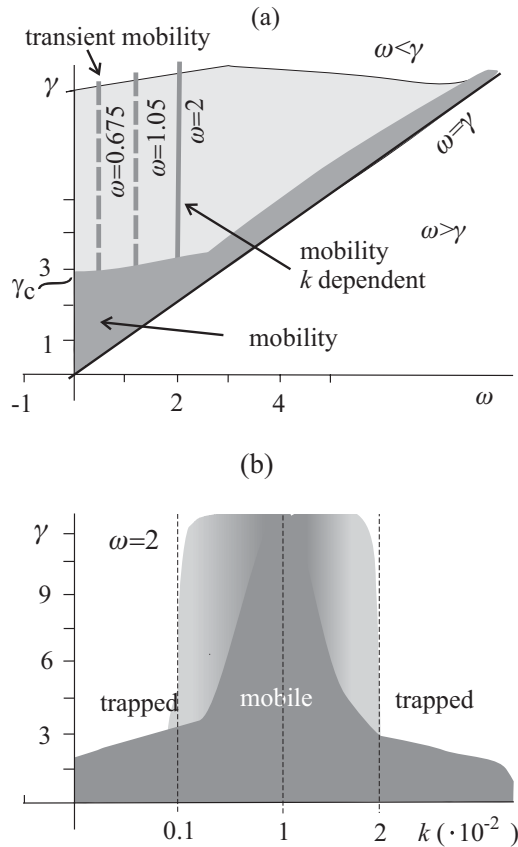
Fig. 2. Bifurcation trapped-moving breather is found in the area around the $\omega = \gamma$ line, in the area $\omega < \gamma < 3$, at $\omega = 0.675$, 1.05 and $\omega = 2$ (a). Mobility of the localized modes with $\omega = 2$ (b). Trapped, transiently moving and moving modes are shown with white, light gray and gray areas, respectively. In all cases the mobility is k and t dependent.

Figures 1 and 2. In the first case, moving breather with constant transverse velocity exists for $0.001 < k < 0.02$. In all other cases, the moving breather gradually radiates energy and finally becomes trapped by the lattice elements. In the present model, radiation is related to the internal mode dynamics of the moving breather (Sect. 2.1) [18] when the internal breather oscillations resonate with the continuous part of the phonon spectrum. The radiation rate of the moving breather depends on ω and the initial transverse velocity k.

The primary interest of this study is focused on the parameter range above the critical curve (Fig. 1), where the cascade saturation mechanism is significant.

3.1 Mapping approach

From the viewpoint of the mapping stability analysis, the breaking of the continuous translational invariance in the lattice systems is associated with the transversal intersections of the stable and unstable manifolds of the fixed point in the origin of the corresponding map [13,20]. The transversal intersections are the seeds for the chaoticity of the map trajectories which is related to the trapping

of the corresponding localized mode by the lattice elements. However, for total power values, P, which correspond to the $\omega \approx \gamma$ and $\omega = 2$, the system integrability is 'recovered', equation (2) [13]. In these cases the stable and unstable manifolds of the fixed point at map origin overlap forming nearly perfect separatrix. Consequently, the effective Pierels-Nabarro barrier vanishes [13] giving a possibility for transverse motion of the localized mode. Note that the zeros of this effective PN barrier do not correspond with the zeros of the PN barrier defined as energy difference between on- and inter-site discrete modes. However, recently an alternative definition of the PN barrier as grand canonical barrier $\Delta G = G_{on} - G_{inter}$ ($G = H - \omega P$) is proposed [28]. Zeros of ΔG correspond to the transparent points obtained by our mapping stability analysis. The initial transverse kick causes the transverse motion of the localized mode with simultaneous excitation of its internal oscillations, which is manifested as a 'breathing' of the moving localized mode.

The breather propagation properties can be interpreted as the result of the breather-lattice interaction, i.e. of the resonance between the breather internal oscillations and environment oscillations (as discussed in references [18] for the case of the DNLS with cubic nonlinearity). This interpretation is supported by the numerical spectral analysis. For example, the power and amplitude spectrums of the moving breathers with low power $P = 0.14$, $k = 0.05$, and high power $P = 21.63$, $k = 0.015$ are shown in Figure 3. In the first case the power spectrum is characterized by single frequency $\omega \approx 9$, and the amplitude spectrum is characterized by a single self-frequency close to 0.1 (the amplitude oscillations of small intensity). In the case of the moving mode with high power, the power spectrum is composed of one main peak around $\omega \approx 1.9$, which is wider than the one in the first case, and additional two satellite peaks with incommensurate frequencies at $\omega_1 \approx 1.60$, $\omega_2 \approx 2.35$. The amplitude spectrum is more irregular with several peaks at frequencies ordered as $1 : 2 : 4 : ...$. It means that the moving breather of small and high P is periodic and quasi-periodic in time [29], respectively (Figs. 3c, 3f).

4 Symmetric collisions

The properties of breather collisions depend on the parameters of colliding breathers (power, velocity, and phase difference), lattice parameters and position of the collision point. In order to simplify complex dependence on the colliding breathers parameters, the study is restricted on symmetric collisions: colliding breathers are identical with opposite velocities $k_1 = k$ and $k_2 = -k$. Two different cases are numerically simulated with respect to the relative position of the collision point, x_0, in the lattice: on-site collisions with x_0 centered on lattice element and inter-site collisions with x_0 centered between two neighboring lattice elements [10]. Therefore, the properties of the symmetric breathers collisions depend on the system parameters P, ω, k, γ, which are mutually interconnected.
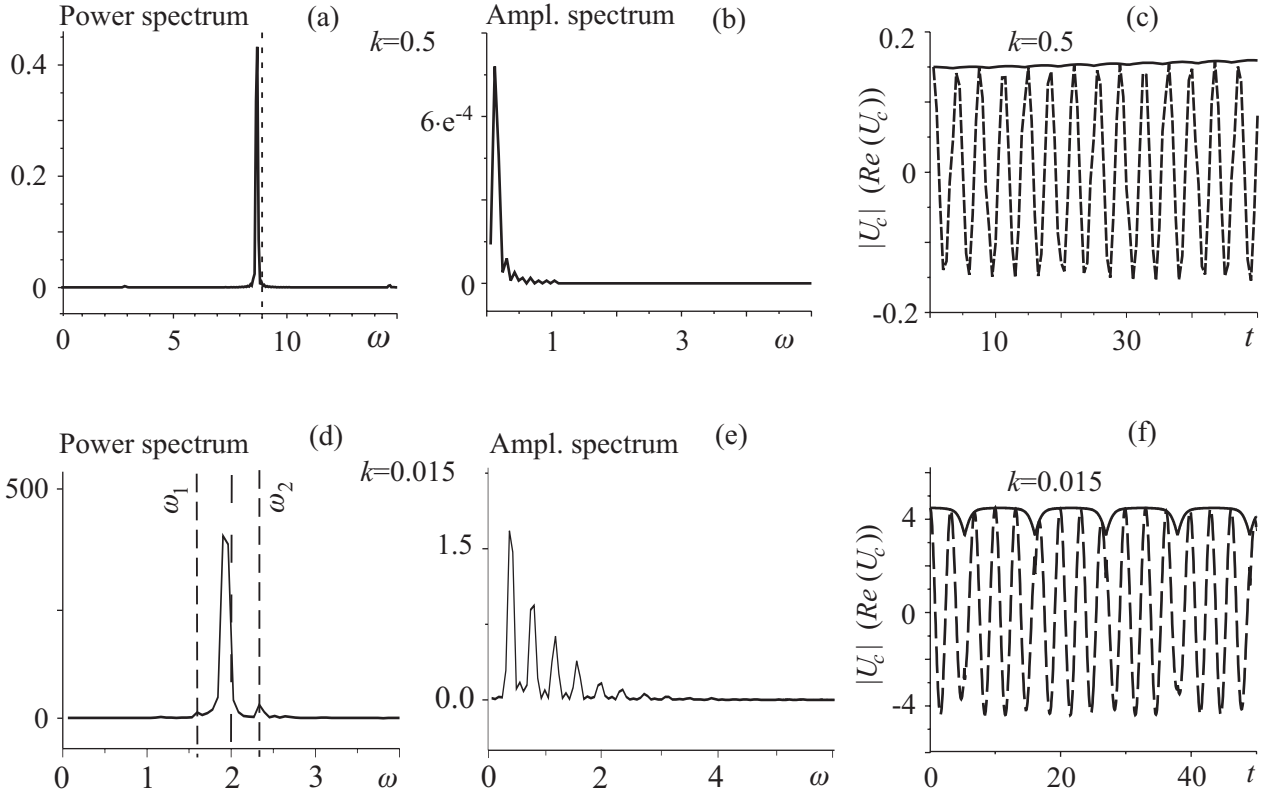
Fig. 3. The power spectrum (a), (d), amplitude spectrum (b), (e), Re(U_c) (dashed curve) and $|U_c|$ (solid curve) against t (c), (f). Parameters are $\gamma = 9.1$, $\omega = 9$, $P = 0.14$, $k = 0.05$ (a)-(c) and $\omega = 2$, $P = 21.63$, $k = 0.015$ (d)-(f). The index c notes the center of breather. In plot (d) the frequencies of the satellite peaks are $\omega_1 = 1.60$ and $\omega_2 = 2.35$.

4.1 On-site and inter-site collisions

Generally, in the whole region of the moving breathers existence, by fixing the transverse velocity k, the increase of the total power changes the type of on-site collision from elastic, Figure 4a, through inelastic with formation of bounded state after multiple collisions, Figure 4b, to the fusion of colliding breathers, Figure 4c. Considering the area above the curve γ_c in Figure 5, in the region of very low powers (where the PN barrier vanishes) the breather collisions are always elastic, Figure 4a.

The properties of the on-site collision, in the region of critical P for $\gamma > \gamma_c$ (border of the gray area in Fig. 5), depend on the colliding breathers transverse velocity k. This region is characterized by the small finite value of the $H_{on} - H_{inter}$ near the first zero of the energy difference (see Fig. 1 in [12]). The colliding on-site or inter-site breathers form bounded state after multiple collisions for small k, or continue transverse propagation across lattice for high k. Relating the value of k to the breather kinetic energy, the observed behavior can be interpreted as follows. Trapping by lattice elements or transverse propagation occurs when kinetic energy of colliding breathers is lower or higher than the corresponding PN potential barrier of the lattice, respectively.

In the lattice with saturable nonlinearity, both on-site and inter-site symmetric collisions of two breathers with high power finally result into the breathers fusion, Figure 4c. The created collision complex, after transient energy exchange between the collision complex and lattice, is trapped by the lattice. During this transient phase the collision complex with power P and energy H relaxes towards more stable configuration with the same power and lower energy H_s. For given P, the value of H_s is estimated as the lower one between energies of the corresponding stationary on-site and inter-site localized modes, i.e. $H_s = \min(H_{on}, H_{inter})$ (Figs. 4b, 4c). As a consequence, the trapping center is on the lattice element when $H_s \approx H_{on}$, or between two neighboring lattice elements when $H_s \approx H_{inter}$. However, the position of the trapping center in the lattice is departed from central lattice position (asymmetry in collision output in Figs. 4b, 4c). This is a result of the sensitivity of the collision complex, initially formed at the maximum of the phenomenological lattice potential, to small perturbations. Thus, although the system is symmetric, the presence of small perturbations (numerical noise) induce asymmetries in collision output. This behavior is consistent with the consideration in Section 3.1. and requires additional analysis.

The region around the γ_c curve in Figure 1 is 'marginal' with respect to the type of collisions. For on-site
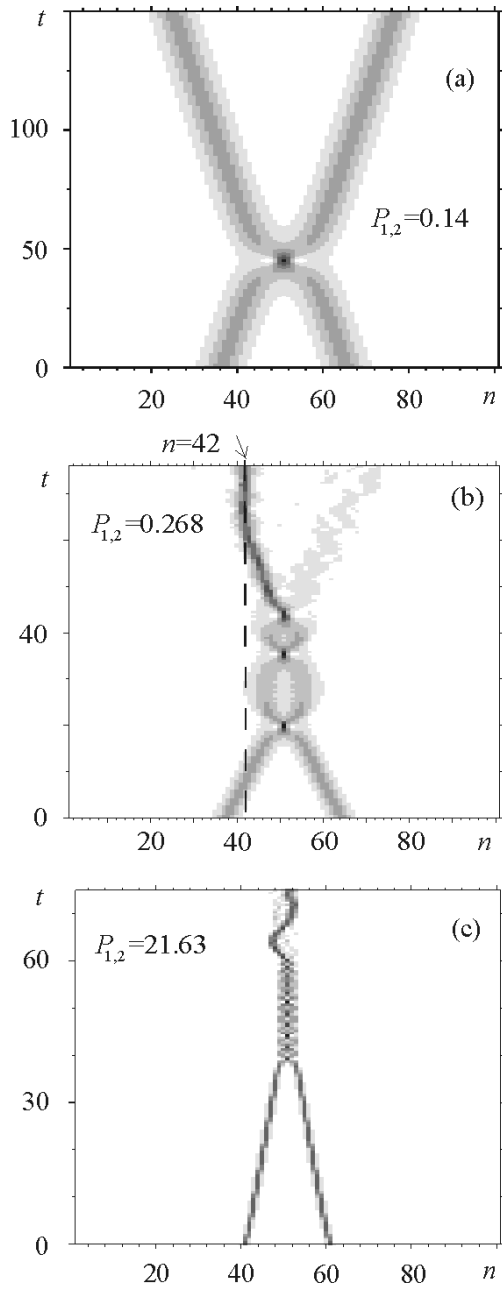
Fig. 5. The P against parameter ω as in figure 1. The moving breathers are observed for the critical values of parameter ω marked by the straight lines, and in the gray region. The dotted curve corresponds to the γ_c in Figure 1. The characteristic types of symmetric collisions are illustrated in boxes. Arrow shows direction of increasing k.

Fig. 4. On-site elastic (a) and inelastic (b), (c) collisions between two moving breathers. For all cases $k = 0.015$. Collision complexes formed after inelastic collisions with $P = 2P_{1,2} = 0.536(b), 43.26(c)$ and $H = 2H_{1,2} = 9.64(b), 216.89(c)$ radiate energy and finally are trapped on lattice element (b) or between two neighboring lattice elements (c). Final state is characterized by the same power P and lower energy, $H_s \approx 9.25(b), 189.33(c)$.

collisions of the moving modes with the $P(\omega)$ curve below the critical curve in Figure 5, the increase of k changes the collision outcome from the bounded state of two colliding modes, through the pair of the unchanged colliding modes, towards breather fusion or breather creation [14,16,17,30] (the last outcome is observed only for high P), Figure 6.
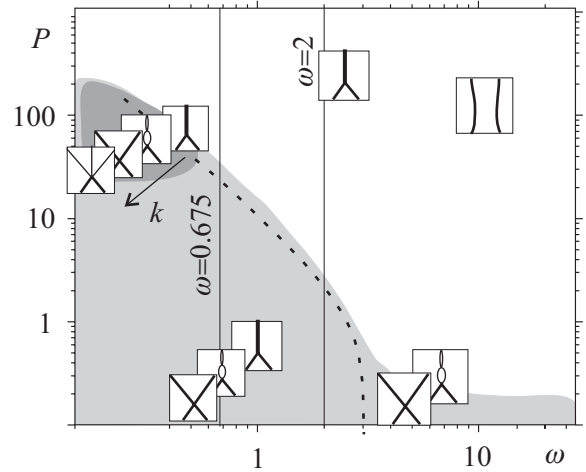
Beside the fusion of two breathers with high power, the inter-site symmetric collisions of two small power breathers can result in a quasi-elastic collisions, Figure 7a. For the critical power, inelastic collision results in a creation of two non identical breathers, Figure 7b. Asymmetric energy redistribution between colliding breathers during the collision process can be related to the numerical noise (which emulates noise in the real physical system) as mentioned above in connection with breather fusion. However, additional investigations are necessary.

4.2 Collision complex

The total power and energy of the collision complex depend on the radiation rate of the moving breathers and the starting time of the collision, which is, on the other hand, a function of initial mode positions and breathers velocity k. In this paper the numerical calculations for all parameter sets show that the collision complex power and Hamiltonian are approximately given as $P \approx P_1 + P_2$ (the relative variation $\delta P \approx 10^{-6}$) and $H \leq H_1 + H_2$ (the relative variation $\delta H \approx 10^{-3}$), respectively. The collision complex is transient localized structure formed by two breathers, Figure 8. Depending on the total power the collision complex can evolve into a pair of moving breathers (elastic collision), a pair of moving breathers with the additional moving/standing breather, or a single breather trapped on/between the lattice elements, Figure 5.

The time period of the collision complex existence can be taken as the characteristic of the collision process. Roughly, when the cascade mechanism of saturation governs the system behavior, the existence time for fixed k depends on P. It is short for very low P, increases with the increase of P and tends to infinity for the moving breathers with high P. The first case corresponds to elastic collisions, and
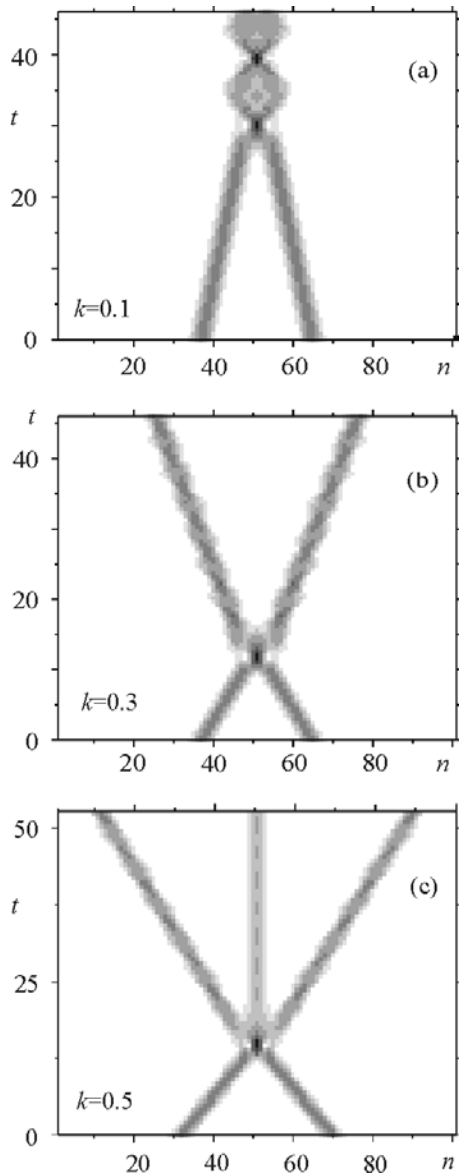
Fig. 6. The (on-site) collision of two identical breathers (initially on-site solitons) with $P = 70.28$, $\omega = 2$ and different k.

Fig. 7. The inter-site collisions (x_0 is in the middle between $n = 50$ and $n = 51$): quasi-elastic, $P_{1,2} = 0.14$, $k = 0.5$ (a), and inelastic with two non-identical breathers after collision, $P_{1,2} = 0.268$, $k = 0.015$ (b).

the last to inelastic collisions, i.e. the colliding breathers fuse.

In the previous section, the type of the breathers collision is commented with respect to the energy exchange between the collision complex and lattice. However, it is only a rough description of the breathers interaction because the internal mode dynamics is not explicitly considered. Its significance can be illustrated by observing the power and amplitude spectrums of the localized structures during the collision process.

After elastic collisions the power spectrum of the resulting breathers contains one peak, as before collision. With the increase of k the peak becomes slightly wider and the amplitude changes from a periodic into a quasi-periodic in time.
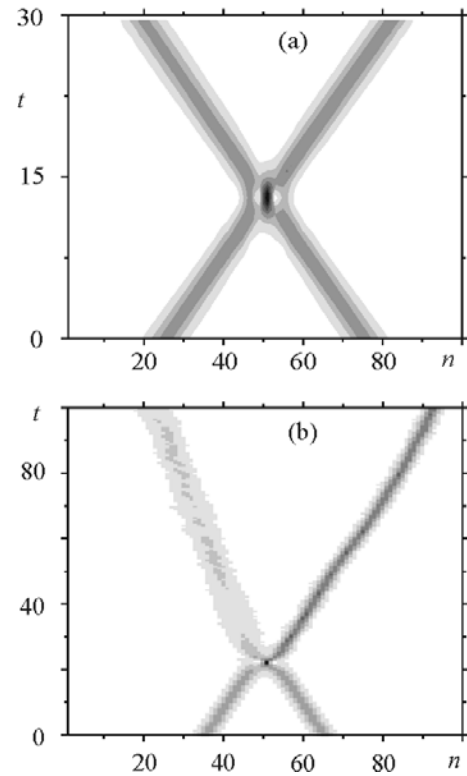
The inelastic collisions result in a formation of a new, trapped breather. Its power spectrum is wider in comparison to the spectrum of colliding breathers. Except the broad spectral peak around $\omega = 2$ additional peak appears around $\omega = 1.2$, Figure 9a. The corresponding amplitude spectrums are shown in Figure 9b. With the increase of k the amplitude spectrum is wider and new incommensurate frequencies appear. Generally, the quasi-periodic or chaotic breathers are indicated by the numerical calculations. In addition, the maximum amplitude of breathers after collision changes from periodic/quasiperiodic to irregular function of time, as illustrated in Figure 8b.

A significant tendency can be observed here: with increasing complexity of the internal structure of the colliding breathers the collision type changes from elastic to inelastic.

At the end of this section it is worth to point out that the present analysis covers the whole parametric space. It completes the earlier attempts to clarify the properties of the symmetric breather collisions in lattices with saturable nonlinearity based on the numerical analysis with fixed breather and lattice parameters [16]. In addition, it clarifies the breather fusion as the only collision output in the lattice system in the region of high power, which is not observed in the continuous systems with saturable nonlinearity [14,15].
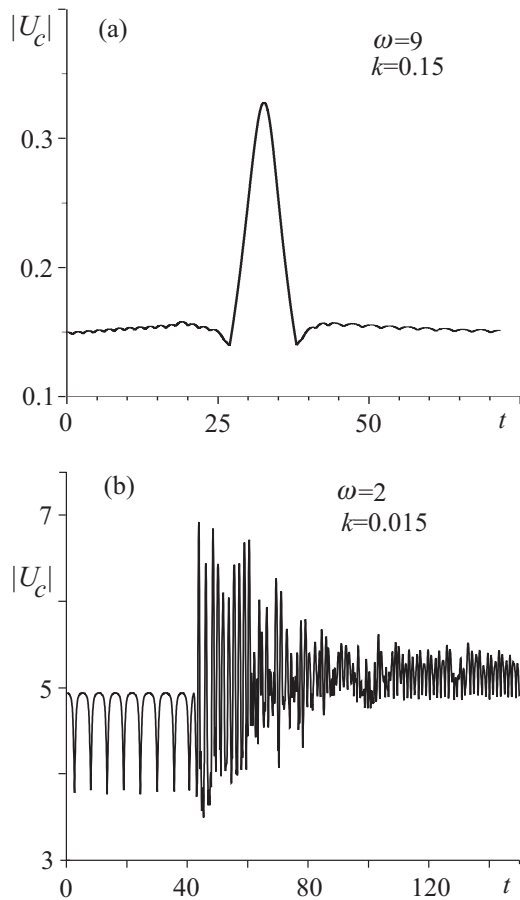
Fig. 8. The maximum amplitude of the breathers against time. The collision complex is created at the collision point. (a) Elastic collision of two breathers with $P = 0.14$. (b) Two breathers with high power $P = 21.63$ fuse into new breather with approximately $P \approx 2 \cdot 21.63$.

Fig. 9. The power (a) and amplitude (b) spectrums before collision (solid curves) and after collision (dashed curves) for colliding breathers with $P = 21.63$, $k = 0.015$. The result of collision is breather merging.

5 Conclusions

This paper is devoted to the study of symmetric collisions between discrete breathers in a lattice with saturable nonlinearity. The properties of breather collisions are strongly correlated with the parameters of colliding breathers (power, transverse velocity), the lattice parameters and position of the collision point. Therefore, several different types of collision are observed in wide parameter space: elastic (quasi-elastic) on-site (inter-site) collision, breather creation, fusion of colliding breathers and creation of two asymmetric breathers (after inter-site collision).

The specific characteristic of the discrete lattices with saturable nonlinearities is the existence of the moving localized modes with high power. However, contrary to the corresponding continuous systems, moving localized modes with high power exist only for a few values of the breathers total power and transverse velocity. The collision of two discrete breathers with high power always results into a breathers fusion.
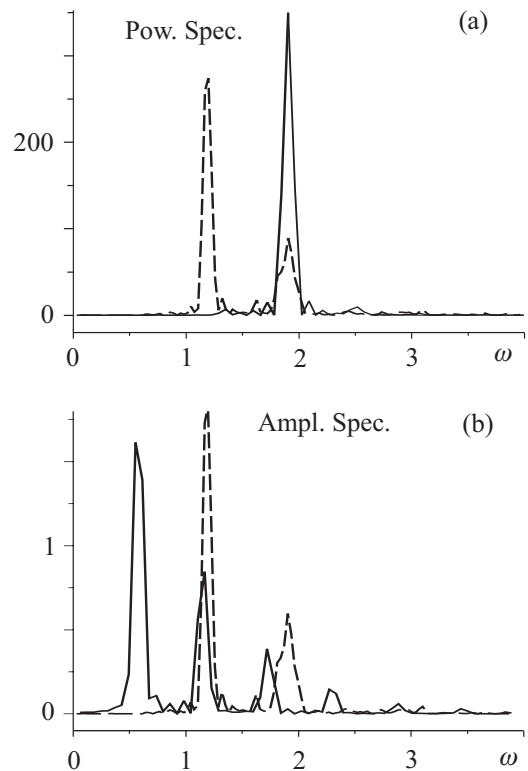
The diversity of the collision outputs is related to the internal structure of the colliding breathers, and the energy exchange between the collision complex and lattice environment. The Fourier analysis of the colliding breathers collision complex shows that elastic and inelastic collisions are results of the interaction between periodic and quasi-periodic breathers, respectively.

Further investigations are necessary for better understanding of asymmetric energy exchange between breathers during collisions and investigation of the phase difference effect on collision. Particularly, the interpretation of localized mode interactions in the language of the dynamics of nonlinearly coupled oscillators will be an intriguing task.

References

1. I.E. Papacharalampous, P.G. Kevrekidis, B.A. Malomed, D.J. Frantzeskakis, Phys. Rev. E **68**, 046604 (2003)
2. Yu.S. Kivshar, D.K. Campbell, Phys. Rev. E **48**, 3077 (1993)

3. M. Peyrard, A.R. Bishop, Phys. Rev. Lett. **62**, 2755 (1989)
4. T. Dauxois, M. Peyrard, A. R. Bishop, Phys. Rev. E **47**, 684 (1993)
5. P.G. Kevrekidis, D.J. Frantzeskakis, R. Carreto-Gonzalez, B.A. Malomed, G. Henning, A.R. Bishop, Phys. Rev. A **71**, 023614 (2005)
6. V. Ahufinger, A. Sanpera, P. Pedri, L. Santos, M. Lewenstein, Phys. Rev. A **69**, 053604 (2004)
7. D.K. Campbell, M. Peyrard, Physica D **18**, 47 (1986)
8. P. Anninos, S. Oliveira, R.A. Matzner, Phys. Rev. D **44**, 1147 (1991)
9. P.G. Kevrekidis, Phys. Lett. A **285**, 383 (2001)
10. S.V. Dmitriev, P.G. Kevrekidis, B.A. Malomed, D.J. Frantzeskakis, Phys. Rev. E **68**, 056603 (2003)
11. M. Stepić, D. Kip, Lj. Hadžievski, A. Maluckov, Phys. Rev. E **69**, 066618 (2004)
12. Lj. Hadžievski, A. Maluckov, M. Stepić, D. Kip, Phys. Rev. Lett. **93**, 033901 (2004)
13. A. Maluckov, Lj. Hadžievski, M. Stepić, Physica D **216**, 95 (2006)
14. W. Krŏlikowski, S.A. Holmstrom, Opt. Lett. **22**, 369 (1997)
15. M.H. Jakubowski, K. Steiglitz, R. Squier, Phys. Rev. E **56**, 7267 (1997)
16. J. Cuevas, J.C. Eilbeck, `arXiv:nlin.PS/0501050v2` 14 Jun 2005
17. A.W. Snyder, A.P. Sheppard, Opt. Lett. **18**, 487 (1999)
18. M. Johansson, S. Aubry, Phys. Rev. E **61**, 5864 (2000)
19. D. Hennig, K.Ø. Rasmussen, H. Gabriel, A. Bülow, Phys. Rev. E **54**, 5788 (1996)
20. D. Hennig, G.P. Tsironis, Phys. Rep. **307**, 333 (1999)
21. M.J. Ablowitz, J.F. Ladik, J. Math. Phys. **17**, 1011 (1976)
22. A.A. Sukhorukov, Yu.S. Kivshar, H.S. Eisenberg, Y. Silberberg, IEEE J. Quantum Electronics **39**, 31 (2003)
23. R.S. MacKay, S. Aubry, Nonlinearity **7**, 1623 (1994)
24. S. Aubry, Physica D **103**, 201 (1997)
25. S. Aubry, Physica D **216**, 1 (2006)
26. W.H. Press, S.A. Teukolsky, W.T. Vetterling, B.P. Flannery, *Numerical Recipes in Fortran 77: the Art of Scientific Computing* (American Institute of Physics, 1997)
27. S. Aubry, Physica D **7**, 240 (1983)
28. T.R.O. Melvin, A.R. Champneys, P.G. Kevrekidis, J. Cuevas, preprint (`http://www.personal.us.es/jcuevas/english.htm`)
29. M. Johansson, S. Aubry, Yu. B. Gaididei, P.L. Christiansen, K.Ø. Rasmussen, Physica D **119**, 115 (1998)
30. D. Chen, S. Aubry, G.P. Tsironis, Phys. Rev. Lett. **77**, 4776 (1996)